A pulse electrochemical deposition method to prepare membrane electrode assemblies with ultra-low anode Pt loadings through in situ construction of active core–shell nanoparticles on an electrode
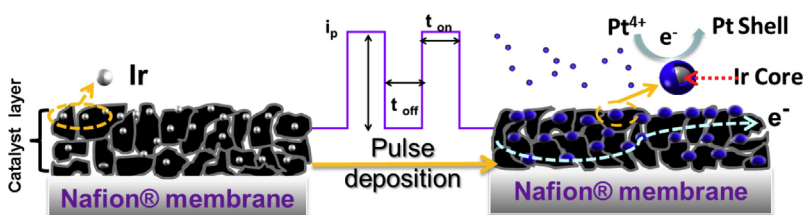
Dai Dang, Shijun Liao*, Fan Luo, Sanying Hou, Huiyu Song, Peiyan Huang

The Key Laboratory of Fuel Cell Technology of Guangdong Province & the Key Laboratory of New Energy Technology of Guangdong Universities, School of Chemistry and Chemical Engineering, South China University of Technology, Guangzhou 510641, China

HIGHLIGHTS

- Novel MEA with low Pt loading of 0.012 mg cm^{-2} at anode prepared by a pulse electrodeposition method.
- Ir@Pt nanoparticles were prepared by in-situ depositing Pt atoms on the Ir/C nanoparticles.
- The MEA shows excellent single cell performance and high Pt utilization.
- The synergetic effect of Pt in shell and Ir in core may result in the ultra-high performance of the MEA.

GRAPHICAL ABSTRACT

ARTICLE INFO

ABSTRACT

Ultra-low Pt loading membrane electrode assemblies (ULP MEAs) are prepared through in situ construction of core–shell Ir@Pt nanoparticles (Ir/Vulcan XC-72R as the core) on the surface of an electrode via a pulse electrochemical deposition (PED) approach. The core material is coated on a membrane with a conventional catalyst-coated membrane process prior to the deposition of the shell metal (Pt in this case). The ULP MEAs are characterized by X-ray Diffraction (XRD), Transmission Electron Microscopy (TEM) and X-ray Photoelectron Spectroscopy (XPS). The effects of a number of preparation parameters on cell performance are investigated in detail. The performance of the ULP MEA, in which the anode loadings of Pt and metals are ∼0.012 mg cm^{-2} and 0.044 mg cm^{-2} (0.012 mg cm^{-2} Pt + 0.032 mg cm^{-2} Ir) respectively, is found to be competitive with that of an MEA prepared with an anode Pt loading of 0.1 mg cm^{-2} (commercial Pt/C catalyst from Johnson Matthey), manifesting the solid advantage of this in situ PED method.

© 2014 Elsevier B.V. All rights reserved.

1. Introduction

Proton exchange membrane fuel cells (PEMFCs) hold great promise for replacement of the currently dominative Lithium-ion batteries and internal combustion engine as power sources with high power density and negative-to-zero environmental impacts [1–5]. Unfortunately, a number of issues still hamper their large-scale application:

(i) relatively high cost due to the use of platinum catalysts, (ii) poor long term operation stability and (iii) adaptation to extreme environments [2,6–8]. However, the main driver for reducing Pt loadings down to really low levels on the anode side is for the really cost-challenging automotive application. Currently, there are two paths to go for Pt usage reduction: one is to synthesize low-platinum catalysts with high Pt utilization [9–12] and another is to develop high-performance MEAs with low platinum loadings [13–18].

In general, the preparation of MEAs with low Pt loadings are conducted by direct deposition of Pt catalysts on the surface of

membrane or back layer, with the aim of the high Pt exposure or dispersion translating through to high Pt utilization in the MEA. The obvious disadvantage of this traditional method is the probable encapsulation or blockage of the active Pt catalyst by the binding materials in MEAs, offsetting the beneficial effect of a larger Pt dispersion. Cavarroc et al. [19] reported a high-performance MEA prepared by directly depositing Pt on the back layer of a MEA using a sputtering technique, the Pt loading in this case was one order of magnitude lower than that in the majority of other studies. Shu and co-workers [20] prepared an MEA by depositing Pt nanoparticles on the back layer of a gas diffusion layer using an atomic layer deposition (ALD) approach, this MEA demonstrated impressive single-cell performance with a power output of 2.95 kW g^{-1} Pt. However, these approaches are difficult to scale up in practical applications due to the harsh demands on the deposition equipment. A pulse electrodeposition method was attempted by Li et al. [21] to prepare MEA with an expectation on Pt crystallite and morphology control by introducing polyethylene glycol (PEG) into the plating bath. However, only a limited success was obtained due to the relative large Pt particles.

Pulse electrodeposition (PED) is becoming an attractive method for decorating materials with unique structures [9,18,22–31]. Recently, the PED method was applied in our laboratory to prepare a core–shell catalyst, in which core nanoparticles were covered by an ultra-thin Pt or Pd shell layer, and achieved acceptable utilization of active metals and cell performance [32]. Motivated by this success, we attempted to prepare MEAs with low platinum loadings through in situ construction of core–shell nanoparticles with a PED method, by which Ir/C is firstly sprayed onto the Nafion® membrane via a conventional catalyst-coated membrane (CCM) process, followed by the pulse deposition of an ultra-thin Pt shell layer on the Ir nanoparticles of Ir/C bonded on the anode catalyst layer. Excitingly, the MEAs prepared with this approach exhibited excellent performance and improved platinum utilization. The performance of a MEA with anode Pt loading of 0.012 mg cm^{-2} is competitive to that of a conventional MEA with anode Pt loading of 0.1 mg cm^{-2}.

2. Experimental

2.1. Fabrication of the Ir/C anode-based MEA

The carbon-supported Ir core was prepared by an organic colloid method previously reported by our group [33]. Briefly, iridium chloride ($IrCl_3$) and sodium citrate were dissolved in ethylene glycol, then Vulcan® XC-72R carbon black was added, followed by stirring for 30 min. The pH of the solution was adjusted to >10 by adding dilute KOH/EG. The mixture was then placed into a Teflon®-lined autoclave and reacted at 180 °C for 8 h, followed by filtering, washing and vacuum drying at 70 °C. For simplicity, we denoted the prepared Ir/Vulcan XC-72R sample as Ir/C.

The Ir/C anode-based MEA, with Ir/C catalyst as the anode was prepared by the following procedures: First, home-made Ir/C (20 wt.% Ir) catalyst was mixed with 5 wt.% Nafion® ionomer solution (DuPont, USA) and isopropanol, then sonicated for 30 min to achieve homogeneous dispersion. The mixture was then directly sprayed onto one side of the membrane, covering an area of 5 cm^2. The weight ratio of the Ir/C catalyst to dry Nafion® was 2.2:1. The Ir loading was 0.032 mg cm^{-2}. For comparison, a carbon-based anode (without Ir) was prepared by the identical process described.

2.2. Preparation of Ir@Pt/C anode-based MEA by pulse electrodeposition

A laboratory set-up was used to prepare the Ir@Pt/C anode-based MEA, which is schematically presented in Fig. 1. The Ir/C anode-based MEA was framed in a fixed area of 5 cm^{-2}, with the Ir/

C anode serving as the working electrode, platinum wire and an Ag/AgCl electrode (3 M KCl) as the counter and reference electrode, respectively. Once a pulse deposition current was applied, Pt was deposited on the Ir nanoparticles to form core–shell structured Ir@Pt. It is worth noting that the Ir/C electrode should be activated before PED by potentiostatic treatment at −0.1 V for 60 s in 0.5 M H_2SO_4 under the protection of N_2, transforming the possible formed oxide film on the surface of Ir nanoparticles into metallic Ir. The current density was fixed at 2.5 mA cm^{-2} for PED. After that, the MEA was immersed in 0.5 M H_2SO_4 at 70 °C for 30 min to remove the possible Cl^- contaminant. The Pt loading of the Ir@Pt/C anode was detected by atomic absorption spectroscopy (AAS).

The cathode was prepared as follows: the catalyst was directly sprayed on the membrane under illumination using 40 wt.% commercial Pt/C (JM4100, Johnson Matthey), yielding a Pt loading of 0.2 mg cm^{-2}. PED Ir@Pt MEA (Ir/C as the substrate or core) was used to denote the MEA prepared with the PED method. For comparison, other MEAs were denoted as PED Pt/C MEA, JM-0.1 MEA (0.1 mg cm^{-2} Pt anode loading), JM-0.012 MEA (0.012 mg cm^{-2} Pt anode loading) and JM-0.044 MEA (0.044 mg cm^{-2} Pt anode loading). JM-0.1 MEA, JM-0.012 MEA and JM-0.044 MEA were prepared totally by using the conventional catalyst coated membrane method, but not the PED method.

The PED Pt/C MEA with an anode Pt loading of 0.012 mg cm^{-2} was prepared by the same procedure as that for the PED Ir@Pt MEA by using XC-72R carbon to substitute Ir/C.

The JM-0.1 MEA, JM-0.012 MEA and JM-0.044 MEA were prepared by the method previously reported by our group [15], using JM Pt/C catalyst for both anode and cathode. The Pt loadings at the cathode were all set to be 0.2 mg Pt cm^{-2} with an only difference at the anode Pt loading, 0.012, 0.044 and 0.1 mg cm^{-2} for JM-0.012 MEA, JM-0.044 MEA and JM-0.1 MEA respectively. The detailed specifications of MEAs prepared in this work were tabulated in Table 1.

2.3. Assembly and measurement of the MEAs

The MEA was assembled by putting gas diffusion layers, which were prepared by spraying a carbon–Teflon® mixture on the pre-treated carbon paper, on the anode and cathode side.

The MEA was tested using a Fuel Cell Testing System (Arbin Instruments, USA). The cell temperature was maintained at 70 °C. H_2 and air, as the fuel and oxidant gas respectively, were fully humidified (100% humidification, hydrogen and air both were set at 70 °C) before feeding with a flow rate of 300 sccm min^{-1} for H_2 and 800 sccm min^{-1} for air. The back pressure for both the anode and cathode was 30 psi.

2.4. Characterizations of the MEAs

The morphology of the Ir@Pt/C catalyst, which was peeled off from the MEA's anode by ethanol, was observed using a high-resolution transmission electron microscope (JEOL JEM-2010HR, Japan) operated at 300 kV. The nanoparticle crystal structure was determined by X-ray diffraction (TD-3500, Tongda, China) using filtered Cu Kα radiation at 40 kV and 30 mA. The 2θ region between 10° and 80° was measured at a scan rate of 4° min^{-1}. The element binding energies were analyzed by X-ray photoelectron spectroscopy (XPS) on a PerkinElmer PHI1600 system (PerkinElmer, USA) using a single Mg Kα X-ray source operating at 300 W and 15 kV. The binding energies were calibrated using the C 1s peak of graphite at 284.6 eV as the reference.

Electrochemical impedance spectroscopy (EIS) and cyclic voltammetry (CV) were performed on a Zahner IM6e electrochemistry station (Zahner, Germany). The measurements were carried out at a
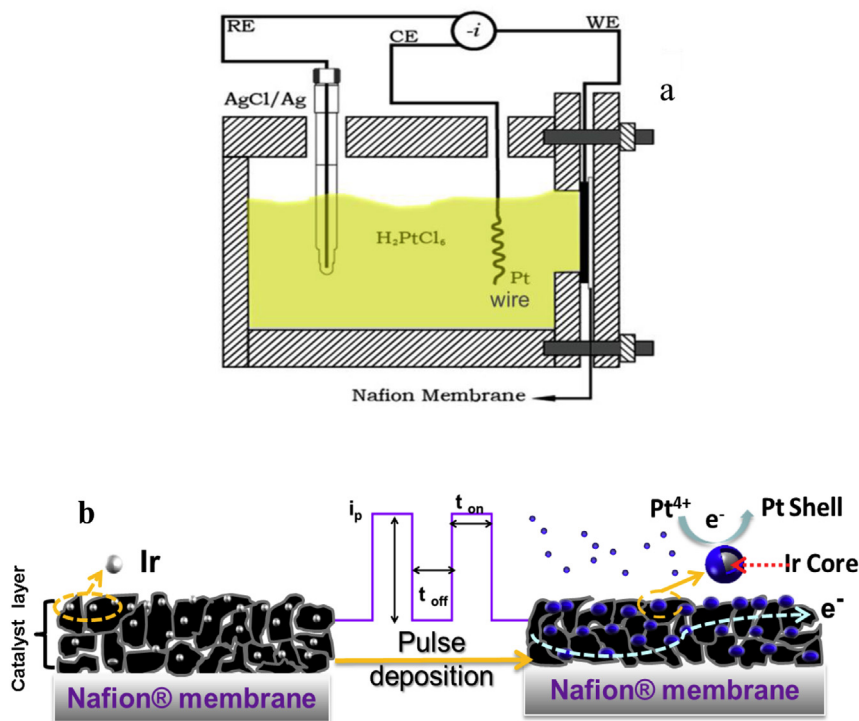
Fig. 1. (a) Schematic illustration of PED setup and (b) in situ formation of core–shell structured MEA through pulse electrodeposition process.

cell potential of 0.8 V with an amplitude of 5 mV and in the frequency range of 0.1–1000 Hz. CV measurements were conducted using humidified N_2 at the cathode (working electrode) and humidified H_2 at the anode.

3. Results and discussion

Fig. 2 shows the XRD patterns of the anodes in different MEAs. The Ir/C prepared in this work, which was used as the core material for further preparation of PED Ir@Pt/C MEA, showed a featureless XRD pattern and this might be explained by a combination of the following deductions: (i) the Ir loading was as low as 0.032 mg cm^{-2}, (ii) the particle size of Ir on the carbon substrate was only $\sim$1.0 nm and (iii) the possible binding effects by Nafion® in the anode layer (blind to X-ray detection). In comparison, the Pt (111) peak at the Bragg angle of 39.6° is clearly detected after PED of Pt, an indication of successful deposition of Pt in this course.

PED deposition of Pt on the MEA with XC-72R carbon black as the only substrate (i.e. PED Pt/C MEA) exhibited a stronger Pt (111) peak than that for the PED Ir@Pt/C MEA with the same Pt loading, implying that the Pt deposited on the carbon substrate has a larger particle size relative to that on the surface of the Ir/C.

The JM-0.1 MEA exhibited somewhat sharper peaks at 39.8° for Pt (111) and 46.2° for Pt (200), relative to PED Ir@Pt/C MEA and PED Pt/C MEA. This result may confirm the advantages of the PED

method, through which ultra-thin Pt layer or small sized Pt were formed. Unfortunately, the mean particle size of Ir@Pt on the PED Ir@Pt/C MEA and Pt on the PED Pt/C MEA could not be calculated because of the weak intensity of the Pt diffraction peak [34]. Furthermore, the refined Pt lattice parameters for the Pt shell of the PED Ir@Pt MEA showed a 3.901 Å f.c.c. lattice constant, which was slightly compressed compared with the JM-0.1 MEA (3.923 Å). In addition, the Pt (111) peak position of PED Ir@Pt/C MEA was slightly shifted to a higher 2θ angle compared to JM-0.1 MEA, in agreement with a similar work reported by Alayoglu and co-workers [35]. It was suggested that this was most probably due to the deposition of extreme thin layer of Pt on the surface of elemental Ir rather than the formation of isolated bulk Pt nanoparticles.

Fig. 3 presents TEM images and their corresponding particle size distribution of Ir/C and Ir@Pt/C. The particles are well dispersed on
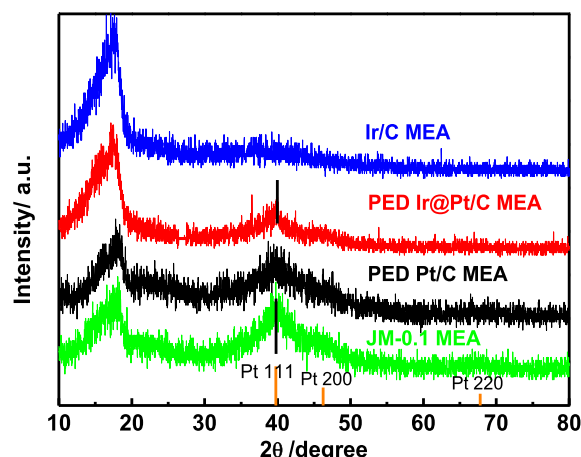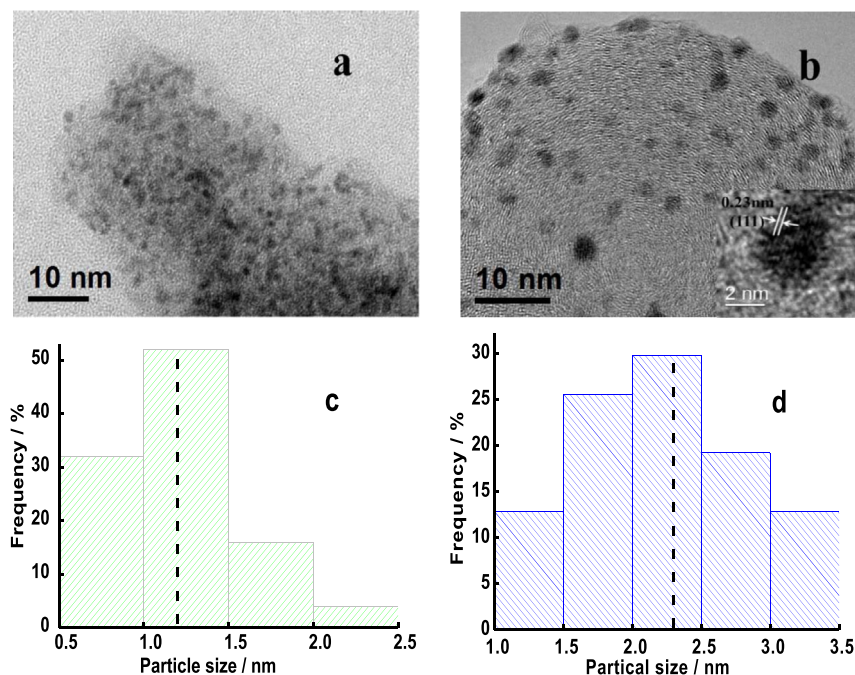
Table 1
The detailed specifications of the five MEAs prepared in this work.

Name	PED Ir@Pt/C MEA	PED Pt/C MEA	JM-0.1 MEA	JM-0.044 MEA	JM-0.012 MEA
Anode Pt Loading/mg cm^{-2}	0.012	0.012	0.1	0.044	0.012
Cathode Pt Loading/mg cm^{-2}	0.2	0.2	0.2	0.2	0.2

Fig. 2. XRD patterns of the anodes of MEAs.

Fig. 3. TEM images and their corresponding particle size distribution diagrams for Ir/C (a, c) and Ir@Pt/C (b, d). The dashed lines indicate the average sizes, which are 1.2 nm in c and 2.3 nm in d, respectively. The insert image in b presents an HRTEM image of Ir@Pt/C catalyst.

the Ir/C and Ir@Pt/C catalysts with tiny particle sizes, these observations confirmed the XRD patterns with broadened Pt diffraction peaks. The high-resolution TEM image in the inset in Fig. 3(b) shows a typical Pt nanoparticle with (111) lattice fringes (0.23 nm). However the boundaries between the Ir core and Pt shell are hardly discernable, which may be attributed to the slight lattice mismatch of Pt and Ir. From the particle size distribution histograms in Fig. 3(c) and (d), it can be seen that the deposition of Pt increased the grain size of Ir from an average particle size of 1.2 nm–2.3 nm Ir@Pt, a good argument to confirm the core–shell structure. The shell thickness could then be calculated to be ∼0.6 nm (i.e. 6 Å), corresponding to less than two layers of Pt since the atomic diameter of Pt is 3.7 Å. Since Pt reduction tends to occur selectively on the metal particles due to similar interface tension between different metals (in this case, Ir and Pt), the Pt deposition on carbon powder is less possible. In the presence of Ir nanoparticles on the support, Pt tends to form a core–shell structure because the interface tension between Pt and Ir is much less than that between Pt and carbon [36].

X-ray photoelectron spectroscopy data was collected to investigate the surface electronic properties and composition of the Ir@Pt/C catalysts. Fig. 4(a), (c) shows the XPS spectra of Ir@Pt/C catalysts for the Pt 4f and Ir 4f core level respectively. In spectral deconvolution it was assumed that the $4f_{5/2}$ and $4f_{7/2}$ lines have the same half widths and the same spin orbit splitting as those of pure Pt. Deconvolution of the Pt 4f spectra in Fig. 4(a) shows two doublet pairs, which are ascribable to metallic Pt and oxidized Pt respectively. The intense doublet at 71.74 eV and 75.06 eV is a signature of metallic Pt (Pt(0)), which is shifted to higher binding energies relative to the monometallic Pt/C catalyst (Fig. 4(b)), with Pt $4f_{7/2}$ at 71.32 eV and Pt $4f_{5/2}$ at 74.62 eV. This was in line with our previous finding [11] and observations reported in other group [35]. It may be explained by the Pt covering of the Ir particles, resulting in increased 5d orbital vacancy.

The Ir XPS spectra in Fig. 4(c), (d) show two doublets, which according to the literature [37], can be ascribed to metallic Ir (74%) and IrO₂ (26%). After Pt deposition, the Ir $4f_{7/2}$ (60.91 eV) and Ir $4f_{5/2}$

(63.9 eV) for the Ir@Pt/C electrode shift to significantly lower binding energies compared with the monometallic Ir/C catalyst (Ir $4f_{7/2}$ at 61.85 eV and Ir $4f_{5/2}$ at 64.86 eV). This might infer the formation of core–shell configuration, in which Pt atoms were electrochemically deposited on the surface of the Ir particles leading to electron transfer from Pt to Ir.

CV as a surface-sensitive technique was used to probe the surface structure and to measure the electrochemical surface area (ECSA). Fig. 5 shows the cyclic voltammograms of PED Ir@Pt/C, PED Pt/C and Ir/C MEAs obtained in a single fuel cell. Although no prominent hydrogen adsorption/deposition peaks can be found from potential ranges from 0.1 to 0.3 V, relative comparisons of ECSAs conclude that the ECSA of Ir@Pt/C is the highest, an indirect proof for its outstanding Pt utilization efficiency. The non prominent hydrogen adsorption/desorption zone in Fig. 5 might be caused by the low Pt loading, leading to relatively high Faradic charging/discharging current aroused from the carbon layer. The occurrence of Pt reduction peak of the PED Ir@Pt/C MEA in the region of 0.6–0.8 V during the reverse scan signifies the Pt shell formation around the It core. It is worth noting that the oxidation peak of the PED Ir@Pt/C MEA was shifted to a higher potential than that of PED Pt/C MEA in the positive going scan, possibly suggesting an interaction between the Ir core and Pt shell.

The influence of t_{on}/t_{off} ratio (i.e. the time ratio between deposition on and off for the PED process) has been investigated, while other parameters remain unchanged to ensure the deposition of the same Pt amount. As shown in Fig. 6, negligible differences in the performance of the PED Ir@Pt/C MEAs are observed in the lower current density end, whereas, striking discrepancies have been found in the higher current density end when the off time increases from 1.5 ms to 12 ms. Experimentally we found that low off time, or high t_{on}/t_{off} ratio, is beneficial for cell performance enhancement. It is hypothesized that better Pt dispersion on the Ir core may be one of the possible origins under these favorable conditions.

The t_{on}/t_{off} was fixed at 3 ms and 1.5 ms to study the effects of the Ir:Pt atomic ratio on the MEAs' performance. It was found that
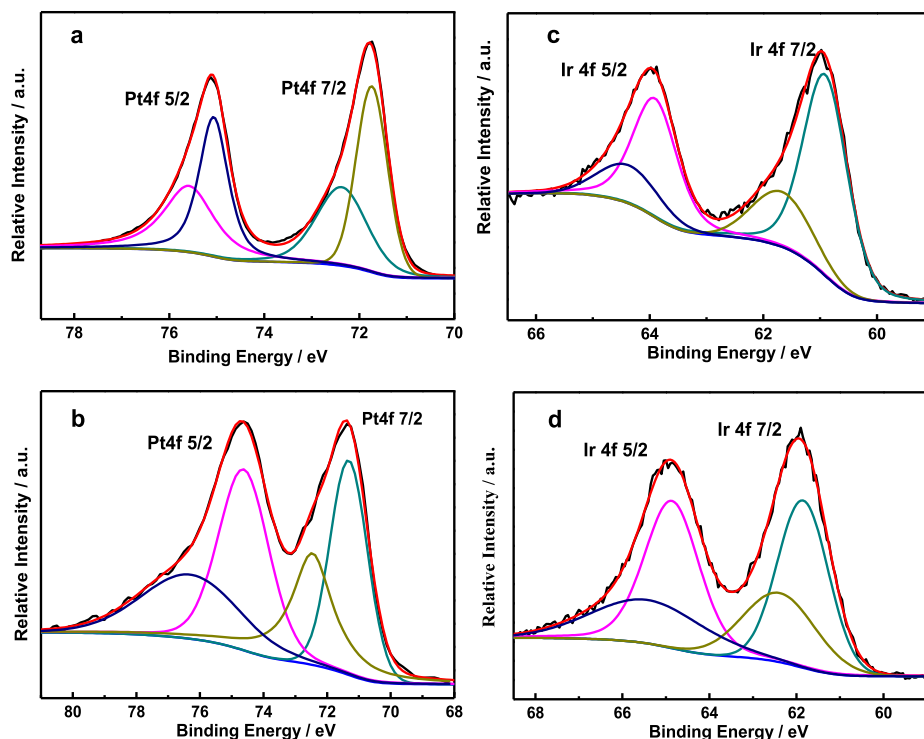
Fig. 4. XPS core-level spectra of the (a) Pt 4f in PED Ir@Pt/C MEA, (b) Pt 4f in JM-0.1 MEA, (c) Ir 4f in PED Ir@Pt/C MEA and (d) Ir 4f in the Ir/C.

the Ir:Pt ratio, or the amount of Pt deposited, significantly affected the performance. As shown in Fig. 7(a), the MEA performance is enhanced with the increasing amount of Pt deposition: the MEA with an Ir/Pt atomic ratio of 0.93:1 (0.035 mg Pt cm^{-2} at the anode) exhibited the best performance whereas the MEA with Ir/Pt ratio of 4.7:1 (0.007 mg Pt cm^{-2} at the anode) resulted in the poorest performance.

Fig. 7(b) shows the performance of the MEAs benchmarked against to the total mass of the metals (Pt + Ir) deposited. The MEA with a Ir/Pt ratio of 2.7:1 (metals laoding: 0.044 mg cm^{-2} at the anode) exhibited the best performance, the mass specific activity of the MEA is as high as 15 kW g$^{-1}_{metals}$. It seems that in this work the atomic ratio of Ir to Pt of 2.7:1 is an optimal one for this type of MEAs.

Fig. 8(a) shows the single-cell performance of MEAs with different anodes. A t_{on}/t_{off} of 3:1.5 was selected for PED process and the Ir/Pt atomic ratio of 2.7:1 was pre-determined based upon the above investigations. It was found that, although the Pt loading for PED Ir@Pt/C MEA is one-tenth that for JM-0.1 MEA, the cell performance is comparable with each other: the cell performance of PED Ir@Pt/C MEA at 0.7 V reaches 500 mA cm^{-2}. Compared with JM-0.044 MEA, in which the anode Pt loading is equal to the anode metals loadings of the PED Ir@Pt/C MEA, the PED Ir@Pt/C MEA still demonstrates superior single cell performance. Meanwhile, in high current density region, PED Ir@Pt/C MEA with relatively low anode Pt loading also outperformed JM-0.1 MEA and JM-0.044 MEA, indicating that the thinner catalyst layer of Ir/C helped to improve the mass transport across the MEA. What's more, once the Pt loading of the JM-0.012 MEA was lowered to the same level as PED
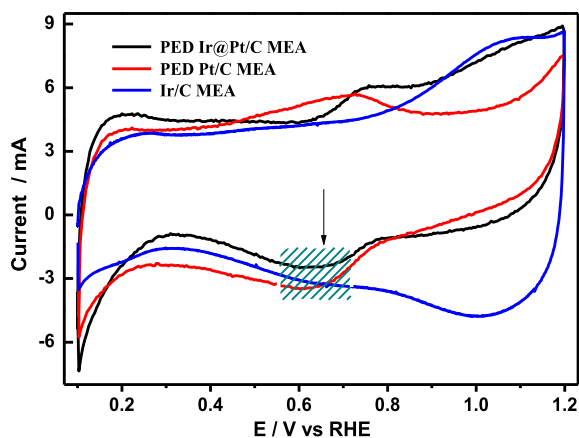

Fig. 5. Cyclic voltammograms of PED Ir@Pt/C MEA, PED Pt/C MEA and Ir/C MEA. The measurements were performed at 27 °C using humidified N$_2$ at the cathode (working electrode) and humidified H$_2$ at the anode (counter electrode and reference electrode). Scan rate: 0.05 V s^{-1}.
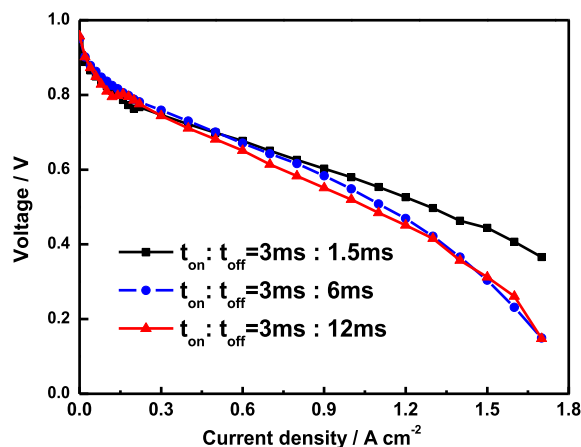

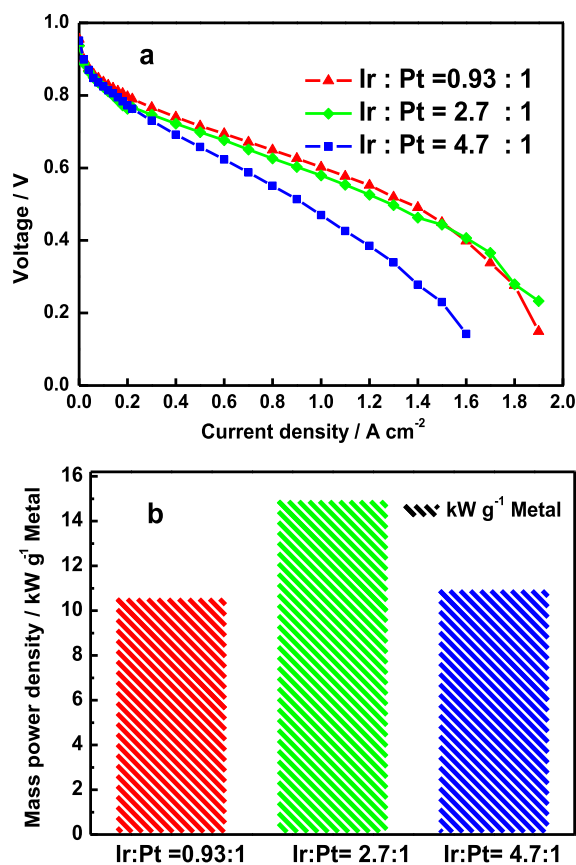**Fig. 6.** Polarization curves of PED Ir@Pt/C MEA at different duty cycles.

Fig. 7. (a) Polarization curves and (b) the mass power density of PED Ir@Pt/C MEA with different Ir:Pt atomic ratios.

Fig. 8. (a) Polarization curves and (b) corresponding bar graphs showing the current density at 0.7 V and the Pt as well as total metal mass power density of different types of MEAs.

Ir@Pt/C MEA (0.012 mg cm^{-2} at the anode), its performance decreased remarkably, only 200 mA cm^{-2} at 0.7 V, indicating the superiority of the in-situ fabricated Ir@Pt/C anode.

There is a big cell performance difference between PED Ir@Pt/C MEA and PED Pt/C MEA, even though they have the same Pt loading (0.012 mg Pt cm^{-2} at the anode). We hypothesized that the following reasons might have caused the above difference: (i) high dispersion of Pt on the surface of the pre-formed Ir nanoparticles, which results in high Pt utilization and performance, and (ii) the possible interaction between the Pt shell and Ir core, which was confirmed by XPS results.

As shown in Fig. 8(b), the mass power density of PED Ir@Pt/C MEA (normalized to the Pt loading) is up to 55 kW g^{-1}, which is much higher than that of JM-0.1 MEA and JM-0.044 MEA. However, if the total metal loading (Pt + Ir) is taken into account, the superiority of PED Ir@Pt/C MEA will be weakened and its mass activity decreases to just 15 kW g^{-1}, however, it is still 2.5 times higher than that of the JM-0.1 MEA and 1.28 times more than that of JM-0.044 MEA, respectively. Considering the price of iridium is only half of platinum, the superiority of PED Ir@Pt/C MEA is still quite distinct. Under this special state, it should be mentioned that the JM-0.012 MEA seems to present the best mass activity of all MEAs although it exhibits very poor single cell performance, of course, this inveracious high mass performance can be mainly attributed to its ultra-low total metal loadings (0.012 mg$_{Pt}$ cm^{-2}). However, if only Pt loading is involved as reference, the mass activity of PED Ir@Pt/C MEA would surpass that of JM-0.012 MEA many times.

Information on the electron and proton conductivity of the MEA was obtained by electrochemical impedance spectroscopy (EIS) measurement, which could help understand (i) the interface
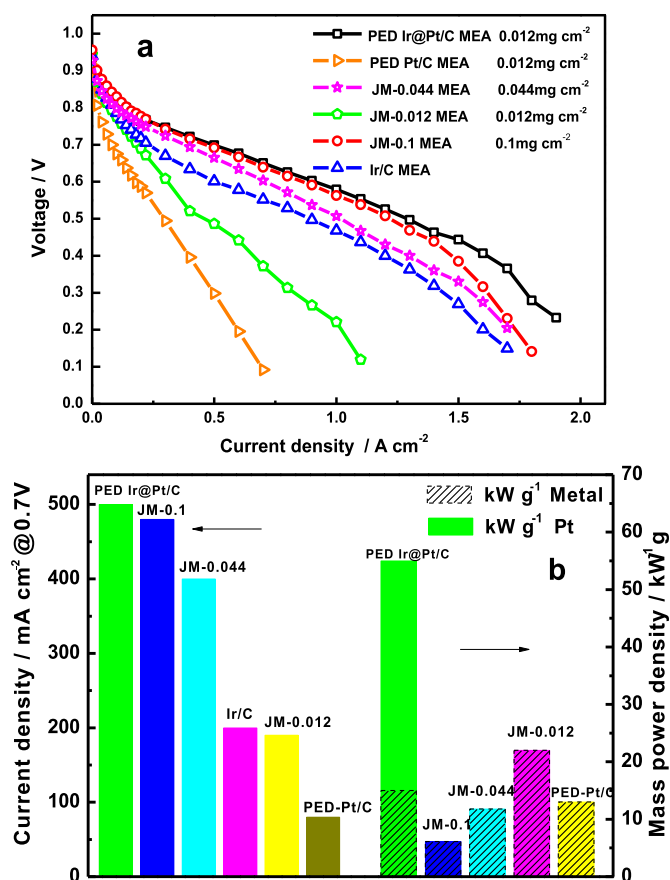
between the catalyst layer and the electrolyte, (ii) the charge transfer rate and (iii) the total contact resistance.

Fig. 9 shows the Nyquist plots of impedance of PED Ir@Pt/C MEA and JM-0.1 MEA at 0.8 V. The high-frequency intercept on the real axis represents the total ohmic resistance of the single cell, which is consisted of the ohmic resistance of the cell components. Generally, the diameter of the arc mainly reflects the charge transfer resistance for the oxygen reduction reaction. However, since the cathode for each MEA have the same composition in this work, thus it is
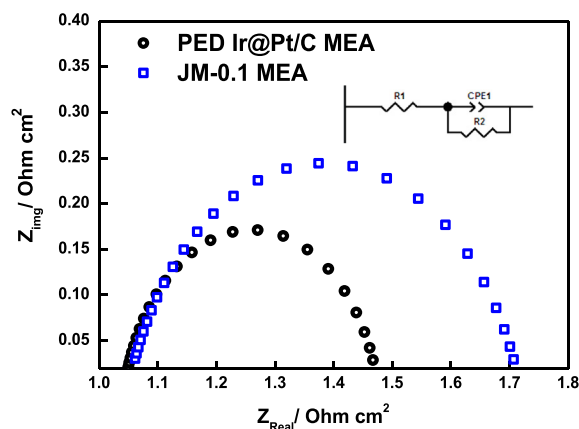

Fig. 9. In situ electrochemical impedance curves of PED Ir@Pt/C MEA and JM-0.1 MEA at 0.8 V. The insert represents an RC equivalent circuit.

Table 2
Resistance of single cell with two types of MEAs.

Sample	PED Ir@Pt/C MEA	JM-0.1 MEA
$R_\Omega(\Omega \text{ cm}^2)$	1.04	1.05
$R_{ct}(\Omega \text{ cm}^2)$	0.43	0.670

reasonable to suggest that the anode process may bring some subtle effects on charge transfer [38,39]. Through simulation with an RC equivalent circuit, cell resistances (R_Ω) and charge transfer resistances (R_{ct}) of the two MEAs could be calculated and are listed in Table 2. It is to be noted that the PED Ir@Pt/C MEA exhibited almost the same ohmic resistance as the JM-0.1 MEA, but the former had a lower charge transfer resistance, which may be one of the reasons for the enhanced single-cell performance presented in Fig. 8. When the cathodes were fixed, charge transfer resistance might be controlled by the proton conductivity and hydrogen permeability limitations. Thus it may reflect on anode process.

4. Conclusion

In conclusion, we prepared a low-platinum MEA by in situ construction of core–shell active nanoparticles using a pulse elec-trodeposition method. The core–shell structure was confirmed by a combination of material and electrochemical characterizations. The MEAs exhibited excellent single-cell performance, its mass activity based on total metals loading is competitive with that of the MEAs prepared with conventional method and with JM Pt/C catalyst (loading: 0.044 and 0.1 mg Pt cm^{-2}) as the anode. We suggest that the enhanced performance of this PED MEA may result from the high dispersion of Pt on the surface of the Ir nanoparticles, the high exposure caused by the in-situ constructed core–shell structure, and the interactions between the ultra-thin Pt shell with the Ir in the core.

Acknowledgments

References

[1] M.K. Debe, Nature 486 (2012) 43–51.
[2] J.S. Spendelow, D.C. Papageorgopoulos, Fuel Cells 11 (2011) 775–786.
[3] S.J. Peighambardoust, S. Rowshanzamir, M. Amjadi, Int. J. Hydrogen Energy 35 (2010) 9349–9384.
[4] A. Rabis, P. Rodriguez, T.J. Schmidt, ACS Catal. 2 (2012) 864–890.
[5] H. Zhang, P.K. Shen, Chem. Rev. 112 (2012) 2780–2832.
[6] R.K. Ahluwalia, X. Wang, J. Kwon, A. Rousseau, J. Kalinoski, B. James, J. Marcinkoski, J. Power Sources 196 (2011) 4619–4630.
[7] H.A. Gasteiger, S.S. Kocha, B. Sompalli, F.T. Wagner, Appl. Catal. B Environ. 56 (2005) 9–35.
[8] R. Borup, J. Meyers, B. Pivovar, Y. Kim, R. Mukundan, N. Garland, D. Myers, M. Wilson, F. Garzon, D. Wood, P. Zelenay, K. More, K. Stroh, T. Zawodzinski, J. Boncella, J. McGrath, M. Inaba, K. Miyatake, M. Hori, K. Ota, Z. Ogumi, S. Miyata, A. Nishikata, Z. Siroma, Y. Uchimoto, K. Yasuda, K.-I. Kimijima, N. Iwashita, Chem. Rev. 107 (2007) 3904–3951.
[9] J. Kibsgaard, Y. Gorlin, Z. Chen, T.F. Jaramillo, J. Am. Chem. Soc. 134 (2012) 7758–7765.
[10] S. Koh, P. Strasser, J. Am. Chem. Soc. 129 (2007) 12624–12625.
[11] H. Gao, S. Liao, J. Zeng, Y. Xie, J. Power Sources 196 (2011) 54–61.
[12] Z. Niu, D. Wang, R. Yu, Q. Peng, Y. Li, Chem. Sci. 3 (2012) 1925–1929.
[13] M. Mougenot, A. Caillard, P. Brault, S. Baranton, C. Coutanceau, Int. J. Hydrogen Energy 36 (2011) 8429–8434.
[14] Y.C. Hsueh, C.C. Wang, C.C. Kei, Y.H. Lin, C. Liu, T.P. Perng, J. Catal. 294 (2012) 63–68.
[15] X. Leimin, L. Shijun, Y. Lijun, L. Zhenxing, Fuel Cells 9 (2009) 101–105.
[16] Z.Q. Tian, S.H. Lim, C.K. Poh, Z. Tang, Z. Xia, Z. Luo, P.K. Shen, D. Chua, Y.P. Feng, Z. Shen, J. Lin, Adv. Energy. Mater. 1 (2011) 1205–1214.
[17] H. Perez, A. Morin, L. Akrour, C. Cremona, B. Baret, J. Haccoun, S. Escribano, A. Etcheberry, Electrochim. Acta 55 (2010) 2358–2362.
[18] W. Zhu, J.P. Zheng, R. Liang, B. Wang, C. Zhang, G. Au, E.J. Plichta, Electrochem. Commun. 12 (2010) 1654–1657.
[19] M. Cavarroc, A. Ennadjaoui, M. Mougenot, P. Brault, R. Escalier, Y. Tessier, J. Durand, S. Roualdès, T. Sauvage, C. Coutanceau, Electrochem. Commun. 11 (2009) 859–861.
[20] T. Shu, S.J. Liao, C.T. Hsieh, A.K. Roy, Y.Y. Liu, D.Y. Tzou, W.Y. Chen, Electrochim. Acta 75 (2012) 101–107.
[21] J. Li, F. Ye, L. Chen, T. Wang, J. Li, X. Wang, J. Power Sources 186 (2009) 320–327.
[22] S. Chen, Z. Wei, H. Li, L. Li, Chem. Commun. 46 (2010) 8782.
[23] H. Kim, N.P. Subramanian, B.N. Popov, J. Power Sources 138 (2004) 14–24.
[24] O.H. Kim, Y.H. Cho, S.H. Kang, H.Y. Park, M. Kim, J.W. Lim, D.Y. Chung, M.J. Lee, H. Choe, Y.E. Sung, Nat. Commun. 4 (2013) 2473.
[25] S. Karimi, F.R. Foulkes, Electrochem. Commun. 19 (2012) 17–20.
[26] C.T. Hsieh, J.M. Wei, H.T. Hsiao, W.Y. Chen, Electrochim. Acta 64 (2012) 177–182.
[27] T. Maiyalagan, X. Dong, P. Chen, X. Wang, J. Mater. Chem. 22 (2012) 5286–5290.
[28] V. Armel, O. Winther-Jensen, R. Kerr, D.R. MacFarlane, B. Winther-Jensen, J. Mater. Chem. 22 (2012) 19767–19773.
[29] C. Kulp, X.X. Chen, A. Puschhof, S. Schwamborn, C. Somsen, W. Schuhmann, M. Bron, Chem. Phys. Chem. 11 (2010) 2854–2861.
[30] C. Coutanceau, S. Brimaud, C. Lamy, J.M. Léger, L. Dubau, S. Rousseau, F. Vigier, Electrochim. Acta 53 (2008) 6865–6880.
[31] L.H.S. Gasparotto, E.G. Ciapina, E.A. Ticianelli, G. Tremiliosi-Filho, J. Power Sources 197 (2012) 97–101.
[32] X. Lu, F. Luo, H. Song, S. Liao, H. Li, J. Power Sources 246 (2014) 659–666.
[33] S. Liao, K.A. Holmes, H. Tsaprailis, V. Birss, J. Am. Chem. Soc. 128 (2006) 3504–3505.
[34] Y. Ra, J. Lee, I. Kim, S. Bong, H. Kim, J. Power Sources 187 (2009) 363–370.
[35] S. Alayoglu, A. Nilekar, M. Mavrikakis, B. Eichhorn, Nat. Mater. 7 (2008) 333–338.
[36] H.L. Skriver, N.M. Rosengaard, Phys. Rev. B Condens. Matter Mater. Phys. 46 (1992) 7157–7168.
[37] F.D. Kong, S. Zhang, G.P. Yin, Z.B. Wang, C.Y. Du, G.Y. Chen, N. Zhang, Int. J. Hydrogen Energy 37 (2012) 59–67.
[38] D. Malevich, E. Hallop, B.A. Peppley, J.G. Pharoah, K. Karan, J. Electrochem. Soc. 156 (2009) B216–B224.
[39] J.R. Kim, J.S. Yi, T.W. Song, J. Power Sources 220 (2012) 54–64.